ELSEVIER

Polymer 43 (2002) 3431–3440

polymer

www.elsevier.com/locate/polymer

Phase identifications and monotropic transition behaviors in a thermotropic main-chain liquid crystalline polyether

Alexander J. Jing[a], Orawan Taikum[a], Christopher Y. Li[b], Frank W. Harris[a], Stephen Z.D. Cheng[a,*]

[a]*Department of Polymer Science, Maurice Morton Institute, The University of Akron, Akron, OH 44325-3909, USA*
[b]*Department of Materials Engineering, Drexel University, Philadelphia, PA 19104, USA*

Dedicated to Professor Imanishi on the occasion of his retirement

Received 16 January 2002; accepted 20 February 2002

Abstract

A thermotropic liquid crystalline (LC) polyether was synthesized by condensation polymerization of 1-(4-hydroxyphenyl-2-(2-methyl-4-hydroxypheyl)ethane) and α,ω-dibromononane, and abbreviated as MBPE-9. Multiple phase transitions were found via differential scanning calorimetry (DSC) upon heating and cooling. Based on wide-angle X-ray diffraction (WAXD) and polarized light microscopy (PLM) experiments, two monotropic LC nematic (N) and smectic phases and three crystalline (orthorhombic K_1, triclinic K_2 and triclinic K_3) phases were identified. A study on kinetics showed that only when the N phase formation rate was faster than the crystallization rate of K_1 phase which directly grew from the melt, the presence of the N phase could accelerate both the overall crystallization and the linear crystal growth rates of K_1 phase. In a narrow temperature region, two distinct crystal growth rates could be observed: one was directly from the isotropic melt, and another was from the N phase.

Keywords: Monotropic phase transition; Phase structure; Main-chain liquid crystalline polyether

1. Introduction

Two experimental observations of phase transformations in thermotropic materials can be identified when more than one ordered phase exists in a system: enantiotropic and monotropic. For a polymer system that contains both crystal and mesophase such as liquid crystalline (LC) phases, enantiotropic LC behavior possesses thermodynamic stability in a temperature region between the crystal melting temperature and the isotropization temperature. Monotropic LC behavior, however, is metastable throughout the entire temperature range. Experimentally, it is only possible to observe monotropic LC phases during cooling in which the crystallization process is bypassed by undercooling due to the kinetically controlled nucleation process. It should be noted that this observation is only possible within the limits of metastability of this phase. The first observation and description of monotropic behavior can be traced as far back as 1877 [1]. From a thermodynamic point of view, one can readily understand the monotropic behavior through a plot of the free energy of the different phases versus temperature as shown in Fig. 1a and b [2–4]. Note that the monotropic phase transition is a broad definition of materials behavior and is not only limited to LC cases: it may also occur between other soft ordered and/or even crystalline phases.

In small molecule liquid crystals, a few examples have been reported which show monotropic LC behavior [5,6]. When the mesogens of these liquid crystals were used to synthesize polymers with methylene spacer units connecting them together, monotropic LC behavior could be retained. One example is 1-(4-alkylphenyl)-2-(4-cyanophenyl)ethane [6] and its polymer analog, synthesized from the coupling of 1-(4-hydroxyphenyl)-2-(2-methyl-4-hydroxyphenyl)ethane with odd-numbered α,ω-dibromoalkanes (MBPE) [7–11], both of which show monotropic LC behavior.

From a view of phase transition kinetics, monotropic LC behavior may exhibit two different crystallization kinetics: namely, crystallization from both the isotropic melt (I) and the LC phase (as shown in Fig. 2). There are three regions in this figure. In region I, the crystal phase grows directly from the I. Region III represents the crystal phase growing from

* Corresponding author. Tel.: +1-330-972-6931; fax: +1-330-972-8626.
E-mail address: cheng@polymer.uakron.edu (S.Z.D. Cheng).

0032-3861/02/$ - see front matter
PII: S0032-3861(02)00159-3

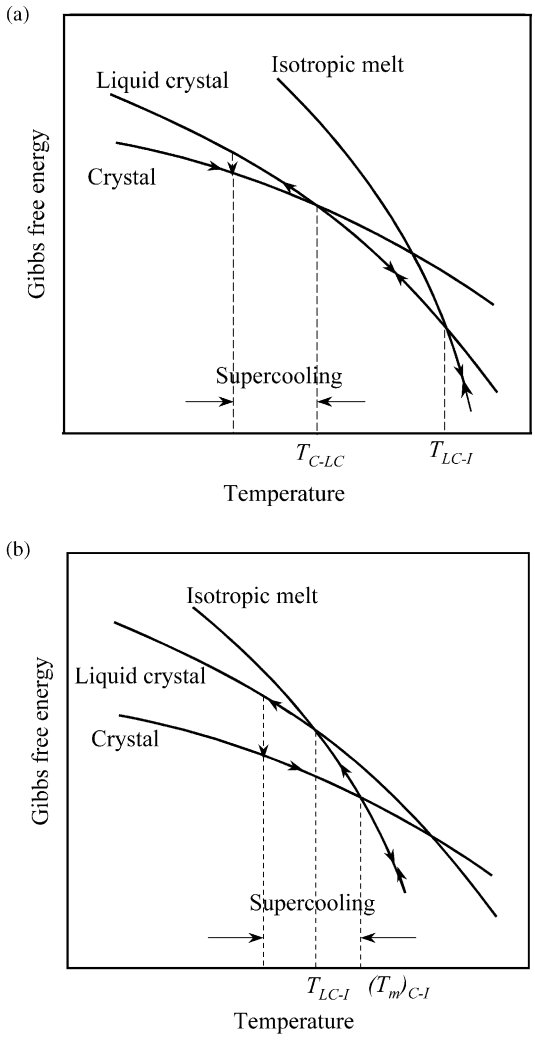

Fig. 1. Gibbs free energy changes with respect temperature at constant pressure for (a) enantiotropic phase transition behavior and (b) monotropic phase transition behavior.

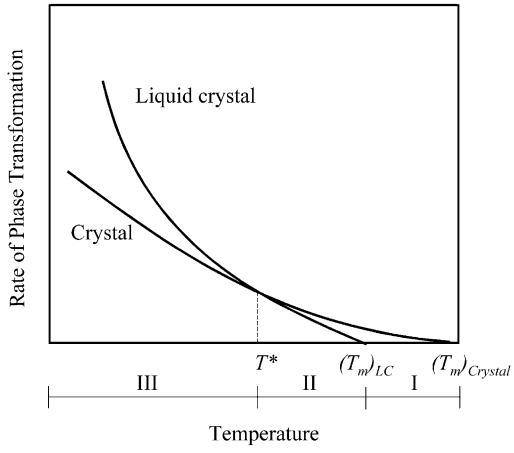

Fig. 2. Phase formation rates versus temperature for the case involving a metastable monotropic phase transition. Three transition regions can be observed.

the LC phase. In region II, both the formation rates of the crystal from the I and from the LC are in the same order of magnitude. Under the condition that the crystal structures formed from the LC phase and directly from the I are identical (in many cases they are not), the region III crystallization from the LC phase is actually a two-step phase transformation process from the I to the crystalline state. Namely, a transition from the I to the LC phase followed by a transition from the LC phase to the crystal phase. Since the monotropic LC phase is metastable over the entire temperature region, it serves as an intermediate step in the crystallization process. One may predict that the crystallization rate from the LC phase should be faster than the rate of crystallization from the I. This is indeed the case for a series of poly(ester imide)s which was recently reported [12–14].

Region II in Fig. 2 is particularly interesting. The simplest case being the molecules are given two choices during the phase transformations and therefore, two possibilities exist: molecules either go to the crystalline phase directly, or they form the LC phase first and then subsequently transform into the crystalline state. If these transformation processes occur on a growth front of the same nucleus in a molecular level, the growth rate for the crystal formed from the I may be significantly slower that that formed from the LC phase. So far experimental observations have not been reported.

In this study, we have chosen a polyether MBPE-9. Although this polymer was investigated since in the early 1990s and reported to show monotropic LC transition behavior [7–11], we are going to focus on their ordered structures and the structure transformation kinetics in the vicinity of the monotropic transition temperature region from both the I and LC phases which have not been previously investigated. The chemical structure of this polyether is:

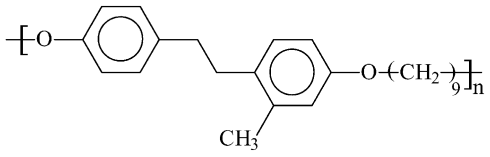

We have found that MBPE-9 shows complicated phase structures and phase behaviors. Two LC phases and three crystal phases have been identified. Both the LC phases are monotropic. As far as we know, this is the first report of a detailed kinetic study in region II where the formation rates of the LC and crystal phases from the I are in the same order of magnitude.

2. Experimental section

2.1. Materials

MBPE-9 was synthesized using condensation polymerization of 1-(4-hydroxyphenyl-2-(2-methyl-4-hydroxypheyl)ethane) and α,ω-dibromononane, following the

published synthetic route [15,16]. Fractional precipitation was used to obtain the material with relatively narrow molecular weight distribution. One MBPE-9 fraction was chosen in this study and had a weight average molecular weight of $M_w = 37\,500$ g/mol, and a polydispersity of 1.24 based on the results of gel permeation chromatography using polystyrene standards.

2.2. Experiments and equipment

Thermal transition properties were studied on Perkin–Elmer DSC7. The temperature and heat flow scales at different cooling and heating rates (2.5–40 °C/min) were calibrated using standard materials. Cooling experiments were always carried out before heating experiments and the cooling and heating rates were always kept identical. The transition temperatures were determined by measuring onset and peak temperatures from cooling and heating scans at different rates. Equilibrium LC transition temperatures were obtained via extrapolations to 0 °C/min.

The kinetic study was carried out by isothermal experiments with TA DSC 2910. Samples were first melted above their melting temperature at 110 °C, and they were then transferred to the DSC cell that was preset to a specific crystallization temperature (T_c) to conduct the isothermal crystallization experiment. In this method an exothermic process could be recorded with respect to crystallization time (t_c). However, when the T_c was high, the exothermic process could not be directly observed using this method due to the prolonged transformation process. Therefore, samples were crystallized at preset T_c for a fixed t_c and then directly heated to 110 °C. The endothermic processes recorded during heating represent the portions of the crystals that had been formed during this period of t_c at the T_c.

One dimensional (1D) wide angle X-ray diffraction (WAXD) powder experiments were performed with a Rigaku 12 kW rotating anode generator (Cu Kα radiation) equipped with a diffractometer. A hot stage was coupled with the diffractometer to study the structural evolution with temperature at constant heating and cooling rates. Sample films having a thickness of approximately 0.1 mm were used and the WAXD patterns were collected by a reflection mode. The temperature was controlled to better than ±0.5 °C. Cooling and heating processes were controlled at 2.5 °C/min to compare with the results obtained by DSC at the same scanning rate. In order to obtain the characteristic profile of different phases, isothermal crystallization was also performed. The sample was first melted at 110 °C, and then quenched to a preset T_c for a prolonged t_c (usually hours to a day) before the WAXD patterns were recorded. The 2θ scanning range was between 1.5 and 30°. When the isothermal experiments were conducted, the 1D WAXD patterns were recorded at a slow scanning rate of 0.5°/min. For the time-resolved heating and cooling experiments, the WAXD scanning rate was 7°/min. Background scattering was subtracted from the sample diffraction patterns.

To identify different phase structures, 2D WAXD fiber experiments were conducted on a Rigaku 18 kW rotating-anode generator (Cu Kα) equipped an image plate. The sample holder was coupled with a hot stage. The temperature was controlled to ±0.5 °C. A 50-min exposure was required for a high quality WAXD fiber pattern. Fibers were spun from the I state and annealed at different temperatures in order to determine phase structure. A typical fiber diameter was 30 μm. Both of the X-ray beams were monochromatized using graphite crystals. The reflection peak positions observed on the 1D and 2D WAXD patterns were calibrated with silicon crystals for known 2θ diffractions and crystallite sizes when $2\theta > 15°$ and with silver behenate for $2\theta < 15°$. The crystal unit-cell determination procedure was based on construction of the reciprocal lattice. Computer refinement was conducted to find the solutions with the least error between calculation values and experimental results [17,18].

Phase morphology and liquid crystalline defects were examined via a polarized light microscope (PLM) (Olympus BH-2) coupled with a Mettler hot stage (FP-90). Isothermal experiments were performed for PLM observation. Thin films of samples were prepared by casting a 1% (w/v) of MBPE–chloroform solution onto a glass slide. Experiments were performed after the solvent had completely evaporated. The thickness of the film is about 10 μm. The linear growth rates of crystals were measured by observing the diameter increase of the growing spherulites (crystals) in different phases.

3. Results and discussion

3.1. Thermal phase transition behaviors

Fig. 3a and b shows two sets of DSC cooling and subsequent heating experiments at different scanning rates. In all the cooling thermal diagrams, the first two exothermic peaks (T_1 and T_2) always take place at 75.5 and 62 °C. The transition temperatures and enthalpies of transitions for these two processes are only slightly cooling-rate dependent. Therefore, they must represent the transitions that are close to thermodynamic equilibrium. In most cases, these transitions are associated with low ordered LC phase transitions. The third exothermic peak (T_3) exhibits a cooling-rate dependence. The exothermic peak temperature changes from 59 to 49 °C and the enthalpy of transition changes from −8.9 to −2.4 kJ/mol as the cooling rates increase from 2.5 to 40 °C/min, respectively. With a further increase in the cooling rate, this exothermic transition became difficult to observe. This undercooling dependence of the T_3 exothermic process suggests that it may be associated with a crystallization process. Around 27 °C, another exothermic process can be

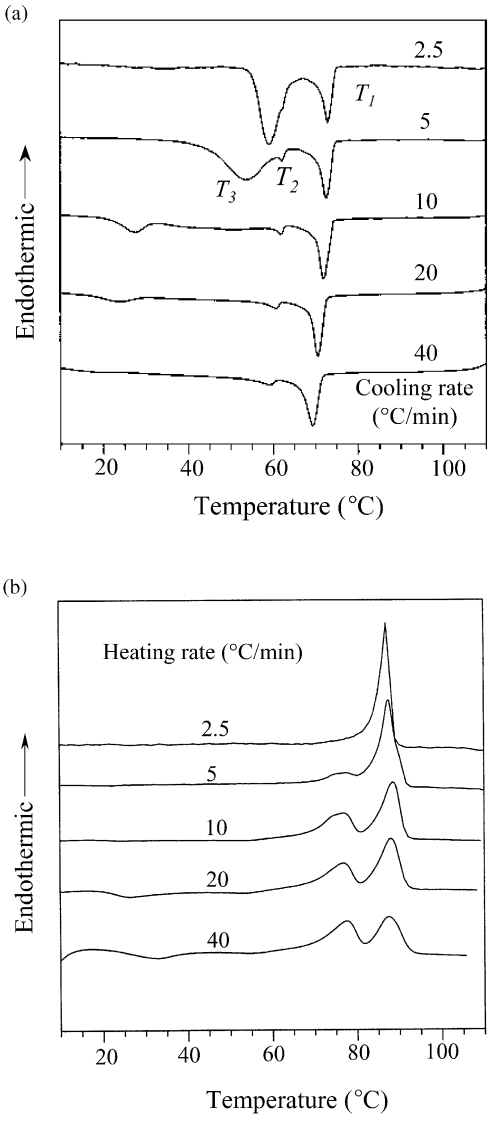

Fig. 3. Two sets of DSC thermal diagrams of MBPE-9 at different cooling (a) and subsequent heating rates (b).

observed when the cooling rates are at 10 and 20 °C/min. This may represent another crystal formation process.

The DSC results, upon subsequent heating at the same rates as cooling experiments, in Fig. 3b exhibit quite different phase transition behaviors from those observed during cooling shown in Fig. 3a. At the slowest heating rate of 2.5 °C/min, only one endothermic peak at ~86 °C is observed having an enthalpy of 15.4 kJ/mol. Based on the shape of the endothermic peak, it is speculated that more than one-transition processes may be involved. This can be further illustrated when the heating rates increased to 5 and 10 °C/min, two transition endotherms are clearly observed (Fig. 3b). At heating rates faster than 10 °C/min, an exothermic process can also be found at low temperatures, indicating that further development of the ordered structure takes place when the prior cooling rates are correspondingly fast.

In order to further examine the differences between these

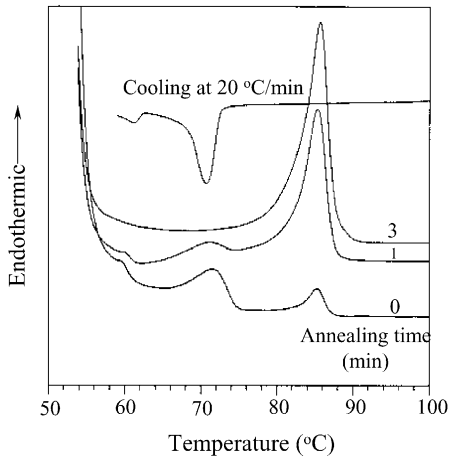

Fig. 4. Set of DSC thermal diagrams of MBPE-9. First the sample was cooled at 20 °C/min to 59 °C, and then isothermally kept the sample at this temperature for t_cs = 0, 1, and 3 min. The samples were then heated to the I state at 20 °C/min.

transition behaviors during cooling and subsequent heating, a specific DSC experiment was designed. The sample was cooled at 20 °C/min from 110 to 59 °C. Note that 59 °C is slightly below the T_2 at 62 °C observed during cooling. The sample was held at an isothermal temperature of 59 °C for different t_cs, followed by heating the sample above the isotropization temperature. The results are shown in Fig. 4. At $t_c = 0$ min, both the T_2 transition at 62 °C and T_1 transition at 75 °C are clearly observed. They are reversible as observed in the DSC thermal diagram during cooling. At 85 °C, however, a new, small endothermic peak appears which represents the crystal melting. This indicates that both the T_1 and T_2 LC phases possess lower transition temperatures than the crystal melting temperature. As a result, both the T_1 and T_2 phases are monotropic and they are metastable with respect to the crystalline phase [3,4]. After only $t_c = 1$ min, the enthalpy of crystal melting (the endothermic peak at ~86 °C) increases continuously and the enthalpies of the T_1 and T_2 phases decrease. After $t_c = 3$ min, neither of the enthalpies of the T_1 and T_2 phases can be observed. Only the crystal melting endothermic peak at 85 °C is observed. This indicates that at 59 °C, the crystal develops rapidly due presumably to the fact that it grows from the precursors of the T_1 and/or T_2 phases.

Although the DSC results show that MBPE-9 possesses complicated phase behaviors, it does not provide any information regarding the phase structural changes. Therefore, structural sensitive methods such as WAXD experiments need to be used to identify the phase changes and determine the phase structures.

3.2. Identification of the phase transitions

Fig. 5a shows a set of 1D WAXD patterns during cooling at 2.5 °C/min. Only an amorphous scattering halo is observed between 97 and 82 °C in the entire 2θ range

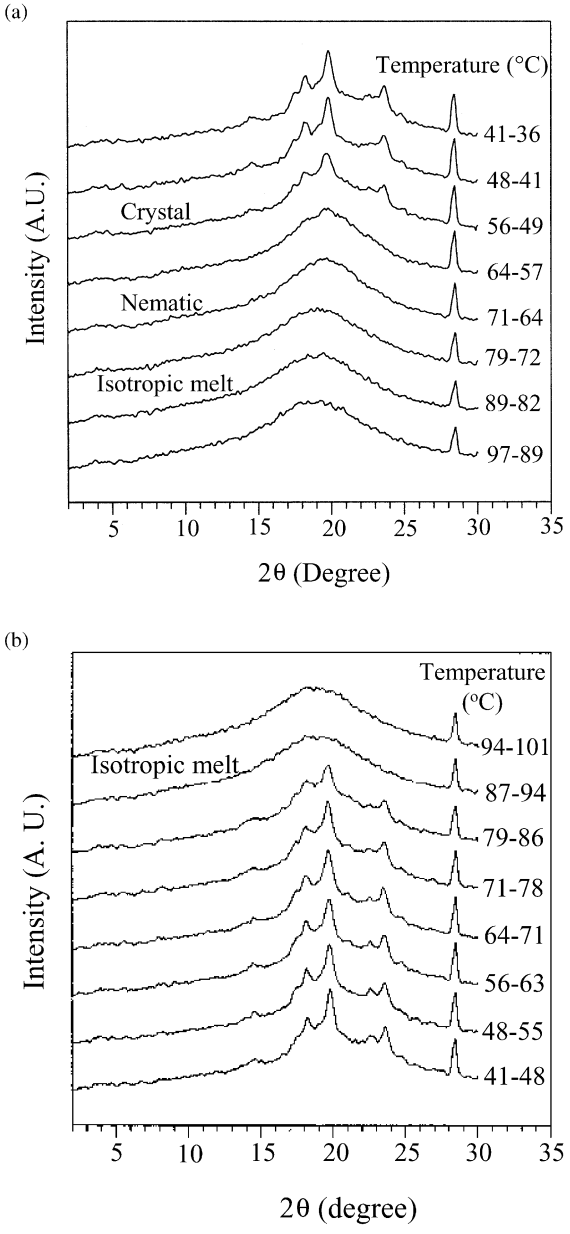

Fig. 5. Two sets of 1D WAXD patterns of MBPE-9 during cooling at 2.5 °C/min (a), and subsequently heating at 2.5 °C/min (b).

between 2 and 35°. Upon further cooling to a temperature region between 79 and 72 °C, a sudden shift of this scattering halo from $2\theta \sim 19$ to ~20° takes place. This is characteristic of the transition from the I to a nematic (N) phase (I → N), as reported in several LCPs [7,10,12–14,19,20]. This corresponds to the T_1 transition observed in the DSC during cooling (Fig. 3a). As temperature is further decreased to below 56 °C, several Bragg reflections in the wide-angle region appear which must be associated with a crystal formation. This structural development corresponds to the T_3 transition at 59 °C in the DSC during cooling (Fig. 3a). However, when the temperature passes through 62 °C (the T_2 transition) the WAXD experiments do not provide any structural changes in the 2θ range between 2 and 35°. Therefore, we conclude that the T_2 phase must possess identical phase structures in a length scale of the lateral chain packing. Although it is possible that the T_2 structure differs in the SAXS region of a nanometer length scale, one can expect that the T_2 phase should be a low ordered smectic phase such as smectic A or C phase. Therefore, a N ↔ S phase transition must exist [7].

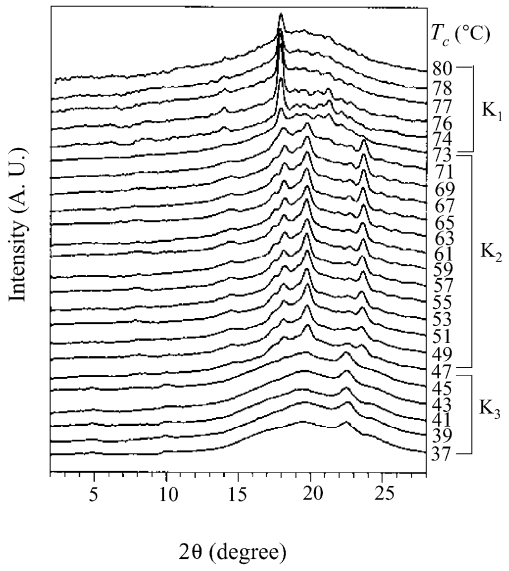

Fig. 6. Set of 1D WAXD patterns of MBPE-9 isothermally crystallized at different T_cs.

Upon heating at 2.5 °C/min, as shown in Fig. 5b, the crystal structure of MBPE-9 melts to the I state at a temperature above 86 °C. Evidence of this can be seen in the sharp Bragg reflections in the 1D WAXD patterns disappearing and returning to the amorphous scattering halo. This agrees with the DSC heating thermal diagrams in Fig. 1b, in which a crystal melting is observed at ~86 °C.

Fig. 6 shows a set of 1D WAXD patterns after MBPE-9 was isothermally crystallized at different T_cs. Three distinct kinds of the WAXD patterns can be categorized: K_1, K_2 and K_3 phases with corresponding T_c regions of 72–80 °C, 48–71 °C and 37–47 °C, respectively. The characteristic reflections for these three phases are: for the K_1 phase, $2\theta =$ 17.9°, for the K_2 phase, $2\theta = 19.8$ and 23.6°, and for the K_3 phase, $2\theta = 22.5$°. It should be noted that the K_1 phase cannot be obtained by non-isothermal cooling and heating since it needs a prolonged isothermal t_c to develop. The K_2 phase can be observed in non-isothermal 1D WAXD experiments when the T_c is below 56 °C (Fig. 5). This corresponds to the T_3 phase transition in DSC results during cooling. The K_3 phase presumably corresponds to the phase transition temperature below 30 °C in the DSC cooling thermal diagrams (Fig. 3).

Because of the existence of these three different crystalline phases in MBPE-9, the sample must undergo phase transformations between these phases via recrystallization

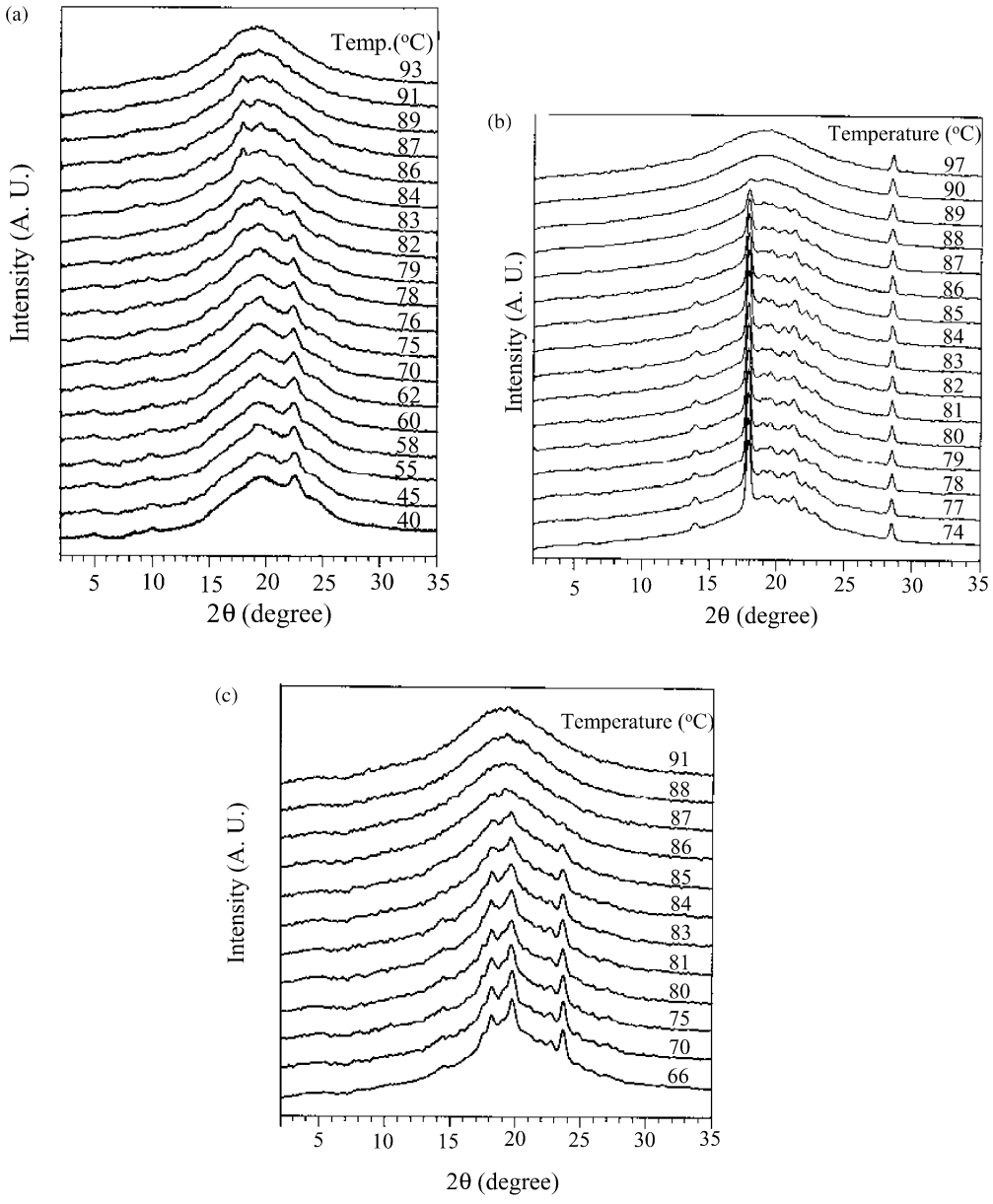

Fig. 7. Three sets of 1D WAXD patterns of MBPE-9 during heating at 1 °C/min after isothermally crystallized at 40 °C from the K3 phase (a); after isothermally crystallized at 74 °C from the K_1 phase (b); after isothermally crystallized at 66 °C from the K_2 phase (c).

and/or reorganization upon heating the sample to the isotropization temperature. Fig. 7a shows a set of WAXD patterns during heating. Starting from the K_3 phase at 40 °C, when the temperature reaches 75 °C, the intensity of the reflection peak at $2\theta = 22.4°$ starts to decrease while the intensity of the reflection peak at $2\theta = 17.9°$ increases. This indicates that the K_3 phase starts to melt at 75 °C and transforms to the K_1 phase, which melts at 86 °C. On the other hand, the melting of the K_1 and K_2 phases are also monitored by 1D WAXD experiments as shown in Fig. 7b and c. During heating, both the K_1 and K_2 phases melt at ~89 and ~86 °C, respectively. The WAXD results do not show that two phases can be directly transformed from one to another.

3.3. Crystal structural identification

Fig. 8a shows a 2D WAXD fiber pattern obtained from the K_1 crystals. The fibers were spun in the I state and then cooled to 76 °C and annealed there for 2 days. Based on the reciprocal lattice, it can be judged that the ($hk0$) reflections are on the equator, while the ($00l$) reflections are on the meridian. Following the standard procedure in determining the crystal lattice, a triangle of ($hk0$) reflections on the equator is constructed. The experimental and calculated d-spacings and reflection angles (2θ) of these diffraction arcs are listed in Table 1. The unit cell of K_1 is determined to be orthorhombic with dimensions of $a = 1.91$ nm, $b = 0.52$ nm, $c = 2.13$ nm, $\alpha = \beta = \gamma = 90°$. Four chains

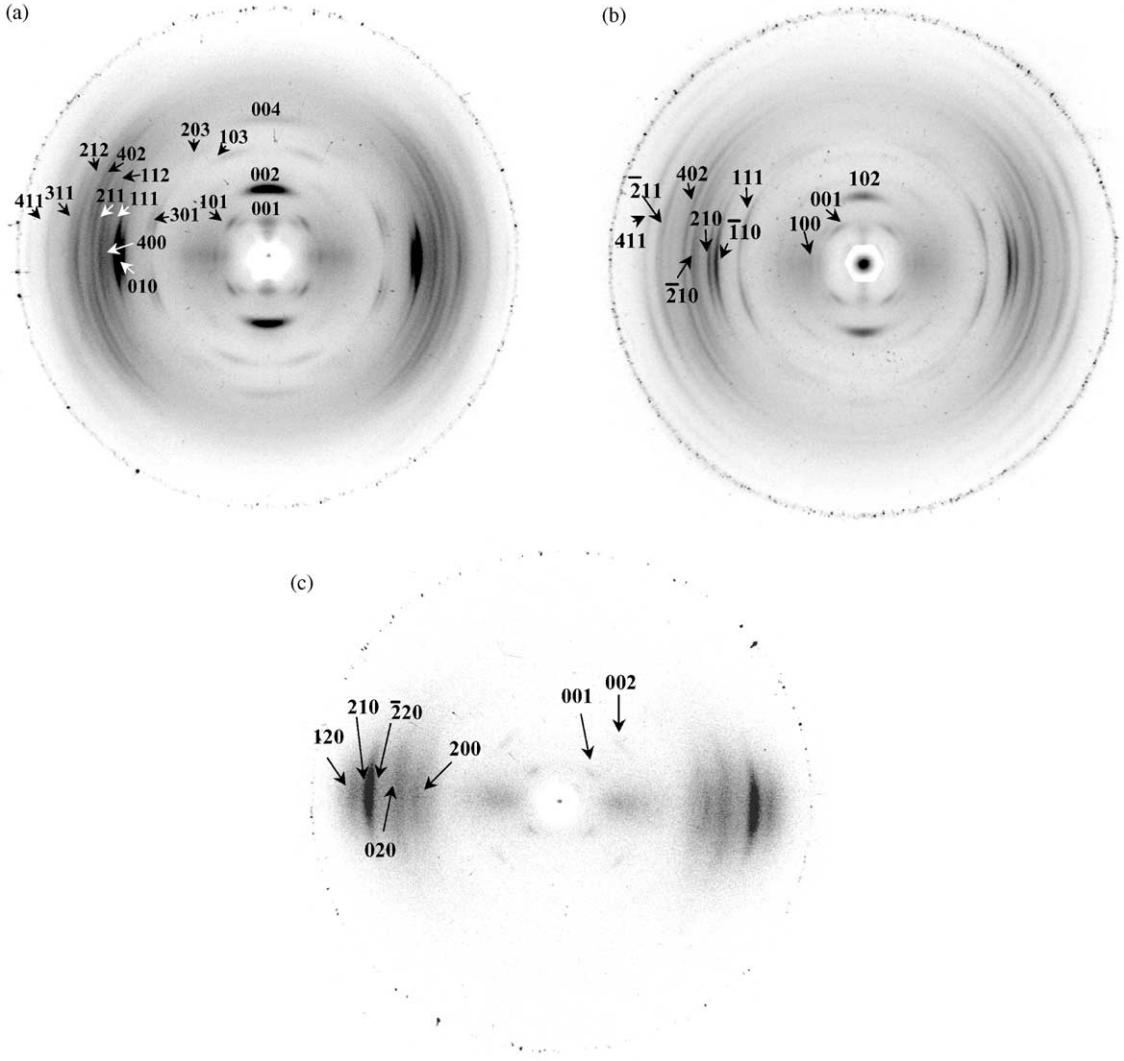

Fig. 8. Three 2D WAXD fiber patterns of MBPE-9 isothermally crystallized at 76 °C for a long time for the K_1 phase (a); isothermally crystallized at 60 °C for a long time period for the K_2 phase (b); isothermally crystallized at 40 °C for a long time period for the K_3 phase (c).

are included in one unit cell and the calculated crystallographic density is 1.11 g/cm^3.

A 2D WAXD pattern containing the K_2 crystals is shown in Fig. 8b. The fibers were spun in I state and then annealed at 70 °C for 4 days. After a detailed analysis of all the reflection arcs, the crystal lattice is identified as triclinic, and its dimensions are $a = 1.84$ nm, $b = 0.622$ nm, $c = 2.19$ nm. $\alpha = 93°$, $\beta = 49.9°$ and $\gamma = 85.5°$. The experimental and calculated d-spacing and reflection angles (2θ) of these reflections of the K_2 crystals are listed in Table 2. The crystallographic density is calculated to be 1.23 g/cm^3, with four chains involved in one unit cell. It needs to be pointed out that in this triclinic unit cell, each motif possesses four chains which are shared by four neighboring repeating units. Therefore, each triclinic cell possesses one motif [21,22].

The K_3 crystal lattice can also be determined based on the analysis of the 2D WAXD pattern in Fig. 8c. Again, the unit cell is determined to be triclinic with dimensions of $a = 1.33$ nm, $b = 0.92$ nm, $c = 2.30$ nm, $\alpha = 89.3°$, $\beta = 50.6°$, and $\gamma = 102.2°$. The crystallographic density is calculated to be 1.12 g/cm^3 with four chains involved in one unit cell (note the issue of the shared chains, and each triclinic cell has one motif [21,22]). The experimental and calculated reflection d-spacing and angles (2θ) of the observed K_3 reflections are listed in Table 3.

3.4. Kinetics of crystallization of the K_1 and K_2 phases

Two different phase transformation kinetics are studied: overall transformation rates and linear growth rates. The overall transformation rates are obtained using isothermal DSC experiments using the reciprocal of half time ($t_{1/2}$) which is equal to the time required for the crystallization to reach the 50% of the maximum transition enthalpy. Fig. 9 shows the overall crystallization rate as a function of T_c. It is important to note that this figure includes crystallization rates of both the K_1 and K_2 phases. The right half of Fig. 9

Table 1
Crystallographic parameters of the K_1 phase in MBPE-9

(*hkl*) plane	2θ (degree)		*d*-Spacing (nm)	
	Exp.[a]	Calcd[b]	Exp.[a]	Calcd[b]
010	17.4	17.1	0.51	0.52
400	18.2	18.2	0.49	0.48
001	4.3	4.2	2.03	2.13
101	6.2	6.2	1.42	1.42
301	14.2	14.5	0.63	0.61
111	18.2	18.2	0.49	0.49
211	19.9	19.9	0.44	0.45
311	22.5	22.5	0.39	0.40
411	25.6	25.7	0.35	0.35
002	8.35	8.3	1.06	1.07
112	19.3	19.6	0.46	0.45
212	21.6	21.2	0.41	0.42
402	20.9	20.4	0.43	0.44
103	13.2	13.3	0.67	0.67
203	15.0	15.5	0.59	0.57

[a] Experimentally observed in Fig. 8a.
[b] Calculated based on the orthorhombic unit cell of $a = 1.91$ nm, $b = 0.52$ nm, $c = 2.13$ nm, $\alpha = \beta = \gamma = 90°$.

above $T_c = 72$ °C is worth noting because only the K_1 phase formed in this T_c range (Fig. 6), and the I ↔ N phase transition occurs at 75.5 °C (see the DSC cooling results in Fig. 3). We can identify three T_c-regimes above 72 °C. In region I (above 75.5 °C), the K_1 phase crystallizes from the I state. However the K_1 phase crystallizes from the N phase in region III (72–73.5 °C) since the N phase is formed at and below 75.5 °C. Again, note that the N phase develops at a much faster rate compared with the K_1 phase due to a lower energy barrier [3,4,14]. In Region II (between $T_c = 73.5$ °C and 75.5 °C), the K_1 phase can be formed from either the I state or the N phase.

It is evident that the K_1 phase that grows from the N phase

Table 2
Crystallographic parameters of the K_2 phase in MBPE-9

(*hkl*) plane	2θ (degree)		*d*-Spacing (nm)	
	Exp.[a]	Calcd[b]	Exp.[a]	Calcd[b]
$\underline{1}00$	6.4	6.4	1.39	1.39
$\bar{1}10$	17.4	16.6	0.51	0.53
$\underline{2}10$	18.3	17.8	0.49	0.50
$\bar{2}10$	20.2	20.6	0.44	0.43
001	5.29	5.3	1.67	1.66
$\underline{1}11$	15.1	15.0	0.59	0.59
$\bar{2}11$	23.5	23.8	0.38	0.37
411	24.9	25.0	0.36	0.36
102	8.4	8.1	1.05	1.09
402	20.8	20.2	0.43	0.44

[a] Experimentally observed in Fig. 8b.
[b] Calculated based on the triclinic unit cell of $a = 1.84$ nm, $b = 0.622$ nm, $c = 2.19$ nm. $\alpha = 93°$, $\beta = 49.9°$ and $\gamma = 85.5°$.

Table 3
Crystallographic parameters of the K_3 phase in MBPE-9

(*hkl*) plane	2θ (degree)		*d*-Spacing (nm)	
	Exp.[a]	Calcd[b]	Exp.[a]	Calcd[b]
200	17.9	18.0	0.50	0.49
$\underline{0}20$	20.0	20.1	0.44	0.44
$\bar{2}20$	23.0	22.9	0.39	0.39
210	23.0	23.0	0.39	0.39
120	24.6	24.3	0.36	0.37
001	5.1	5.1	1.74	1.74
002	10.0	10.1	0.88	0.88

[a] Experimentally observed in Fig. 8c.
[b] Calculated based on the triclinic unit cell of $a = 1.33$ nm, $b = 0.92$ nm, $c = 2.30$ nm, $\alpha = 89.3°$, $\beta = 50.6°$, and $\gamma = 102.2°$.

does so much faster than it does from the I. This can be explained by suggesting that the formation of N phase introduces molecular orientation order, which may have served as precursors for the further development of the K_1 structure. Note that in region II between 73.5 and 75.5 °C, the overall growth rates of the K_1 phase exhibit a sudden change as shown in Fig. 9. It is surprising that the overall crystallization rate of the K_1 phase does not suddenly change at the I ↔ N transition temperature of 75.5 °C. Instead, this sudden change appears at a lower temperature between 73.5 and 74.5 °C. This suggests that as long as the overall rates of the crystal formation from the I are slightly faster than that of the N phase, the overall crystallization rates are dominated by the fast formation process (see region II in Fig. 2). Only after the N phase formation rate becomes faster compared with the overall crystallization rate of the K_1 phase the sudden change of this rate on the K_1 phase can occur. On the other hand, below $T_c = 72$ °C, the K_2 phase

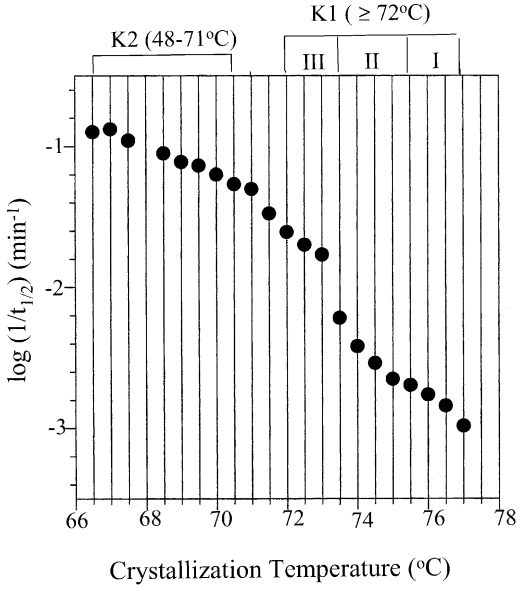

Fig. 9. Overall crystallization rates of the K_1 and K_2 phases in MBPE-9 versus T_c.

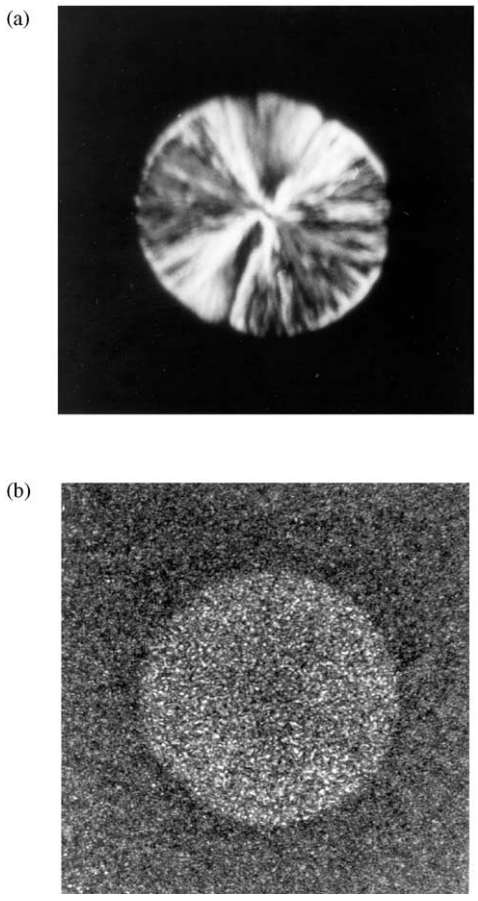

Fig. 10. PLM photographs of MBPE crystals formed at different isothermal crystallization temperatures at 77.5 °C for the K_1 phase (a), at 69.5 °C for the K_2 phase (b).

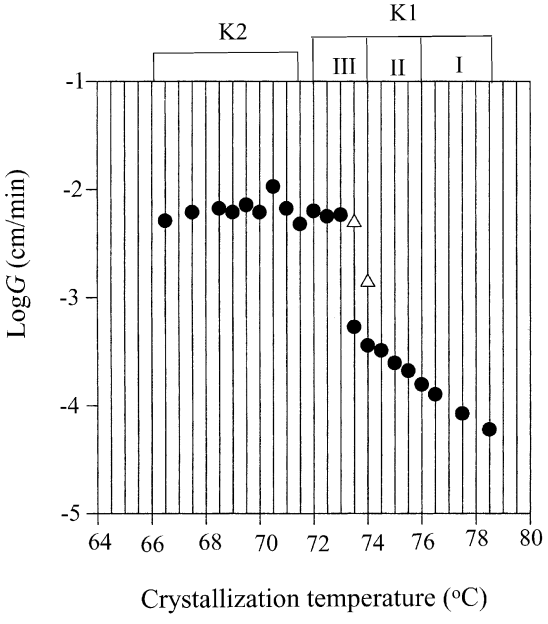

Fig. 11. Linear crystal growth rates of the K_1 and K_2 phases in MBPE-9 versus T_c.

forms. Note that this phase is always developed from the N phase, and the overall crystallization rates gradually increases with decreasing T_c.

The remaining issue to be discussed is that the overall crystallization rate includes both the primary nucleation and crystal growth step. In order to distinguish the effects of these two steps, we need to investigate the linear growth rates (G) in PLM. One necessary condition for this study is that these two crystal phases must exhibit different morphological textures in PLM. When the T_c is 77 °C, the K_1 phase grows and it shows a spherulitic morphology having an irregular maltese cross (Fig. 10a). Upon decreasing the T_c to 69.5 °C (where the K_2 phase develops) the spherulites possesses no maltese cross but have different birefringence compared with the surroundings (Fig. 10b). Therefore, these different textures provide a basis to observe each phase's individual growth rate under PLM.

Fig. 11 shows a relationship between log (G) and T_c for both the K_1 and K_2 phase formations. Above $T_c = 72$ °C, the K_1 phase grows while below this T_c, the K_2 phase forms. In the T_c range where the K_1 phase forms, three regions can be identified in this figure, agreeing with the overall crystallization rates in Fig. 9. Comparing Fig. 11 with Fig. 9, the sudden changes of both rates indicate that not only the linear growth rates exhibit the sudden changes but also the primary nucleation rates do as well. Therefore, it can be deduced that below and above the temperature of these sudden changes, both primary nucleation and growth barriers are different due to the existence of the N precursors. Furthermore, during the sudden change of the linear growth rates in Fig. 11, two growth rates are observed. It is presumed that the faster rate is attributed to the growth from the precursors of the N phase, while the slower one represents a direct growth from the I. Therefore, two growth barriers exist for the linear growth rates even at an identical T_c at which the sudden change of the linear growth rates occurs. In addition, the linear growth rates of the K_1 phase in region III (and those of the K_2 phase at lower T_cs) are essentially invariant. However, in Fig. 9, a continuous increase of the overall crystallization rates of the K_1 (and K_2 phases at lower T_cs) with decreasing T_c is found. This indicates that the increase of the overall crystallization rates must be predominately associated with the primary nucleation rates increasing with decreasing T_c rather than the linear crystal growth rates doing the same.

4. Conclusion

The phase structures of MBPE-9 have been identified. Two monotropic LC phases have been observed upon cooling at 75.5 and 62 °C, respectively. The former one represents the I ↔ N phase transition and the latter one may be associated with the N ↔ S phase transition. In slow cooling, a triclinic crystal K_2 phase formed at about 59 °C. However, in fast cooling, another triclinic crystal K_3 phase appears at

around 27 °C. Formations of the K_2 and K_3 phases are also observed during isothermal crystallization in the temperature ranges of 49–71 °C and 37–48 °C, respectively. The crystalline K_1 phase, which has orthorhombic unit cell, is only obtained by isothermal crystallization at $T_c \geq 72$ °C. The K_1 and K_2 phases melt directly to the I state upon heating, whereas the K_3 phase melts and recrystallizes into the K_1 phase during heating. The crystallization kinetics of the K_1 phase can be divided into three T_c regions due to the interference of the monotropic I ↔ N transition at 75.5 °C. Above $T_c > 75.5$ °C in region I, the K_1 phase grows directly from the I. In region III, where T_c is between 72 and 73.5 °C, the K_1 phase develops from the N precursors. In region II ($73.5 \leq T_c \leq 75.5$ °C), the K_1 phase forms from either the I or the N phase. Furthermore, a sudden change of both the overall crystallization rates and the linear growth rates are found in region II. However, this change does not take place at the I ↔ N transition of 75.5 °C. Instead, it starts at the temperature of 73.5 °C where the formation rate of the N phase exceeds that of the K_1 phase from the I. Based on these experimental observations, it is concluded that the presence of the N phase substantially decreases both the primary nucleation and growth barriers to accelerate the K_1 formation rates.

Acknowledgements

This work was supported by the NSF (DMR-96-17030) and the ALCOM Scientific and Technology Center (DMR-91-57738) at Kent State University, Case Western Reserve University and the University of Akron.

References

[1] Lehmann O. Uber Physikalische Isomerie 1877 (from Keller H. History of liquid crystals). Mol Cryst Liq Cryst 1973;21:1.
[2] Percec V, Keller A. Macromolecules 1990;23:4347.
[3] Cheng SZD, Keller A. Annu Rev Mater Sci 1998;28:533.
[4] Keller A, Cheng SZD. Polymer 1998;39:4461.
[5] Andrews BM, Gray GW. Mol Cryst Liq Cryst 1985;123:257.
[6] Carr N, Gray GW. Mol Cryst Liq Cryst 1985;124:27.
[7] Ungar G, Feijoo JL, Keller A, Yourd R, Percec V. Macromolecules 1990;23:3411.
[8] Percec V, Zuber M, Ungar G, Castillo AA. Macromolecules 1992;25:1193.
[9] Cheng SZD, Yandrasits MA, Percec V. Polymer 1991;32:1284.
[10] Yandrsits MA, Cheng SZD, Zhang AQ, Cheng JL, Wunderlich B, Percec V. Macromolecules 1992;25:2112.
[11] Herberer D, Keller A, Percec V. J Polym Sci Polym Phys Ed 1995;33:1877.
[12] Pardey R, Zhang AQ, Gabori PA, Harris FW, Cheng SZD, Adduci J, Facinelli JV, Lenz RW. Macromolecules 1992;25:5060.
[13] Pardey R, Shen D, Gabori PA, Harris FW, Cheng SZD, Adduci J, Facinelli JV, Lenz RW. Macromolecules 1993;26:3687.
[14] Pardey R, Wu SS, Chen J, Harris FW, Cheng SZD, Keller A, Aducci J, Facinelli JV, Lenz RW. Macromolecules 1994;27:5794.
[15] Percec V, Yourd R. Macromolecules 1988;21:3379.
[16] Percec V, Yourd R. Macromolecules 1989;22:524.
[17] Eashoo M, Wu Z, Zhang AQ, Shen D, Tse C, Harris FW, Cheng SZD, Garder KH, Hsiao BS. Macromol Chem Phys 1994;195:2207.
[18] Li CY, Wang B, Cheng SZD. X-ray analyses in polymers. In: Meyers RA, editor. Encyclopedia of analytical chemistry. New York: Wiley, 2000. p. 8105–24.
[19] Yoon Y, Zhang AQ, Ho RM, Cheng SZD, Percec V, Chu P. Macromolecules 1996;29:294.
[20] Yoon Y, Ho RM, Moon BS, Kim D, McCreight KW, Li F, Harris FW, Cheng SZD, Percec V, Chu P. Macromolecules 1996;29:3421.
[21] Ge JJ, Zhang AQ, McCreight KW, Ho RM, Wang SY, Jin S, Harris FW, Cheng SZD. Macromolecules 1997;30:6498.
[22] Ruan J, Ge JJ, Zhang AQ, Jin S, Wang SY, Harris FW, Cheng SZD. Macromolecules 2002;35:736.